RSC Advances

PAPER

View Article Online
View Journal | View Issue

Cite this: *RSC Adv.*, 2022, **12**, 17466

Uracil derivatives as HIV-1 capsid protein inhibitors: design, *in silico*, *in vitro* and cytotoxicity studies†

Deepthi Ramesh, [a] Amaresh Kumar Mohanty,‡[b] Anirban De,‡[a] Balaji Gowrivel Vijayakumar, [a] Aiswarya Sethumadhavan,[c] Suresh Kumar Muthuvel,[b] Maheswaran Mani[c] and Tharanikkarasu Kannan *[a]

A series of novel uracil derivatives such as bispyrimidine dione and tetrapyrimidine dione derivatives were designed based on the existing four-point pharmacophore model as effective HIV capsid protein inhibitors. The compounds were initially docked with an HIV capsid protein monomer to rationalize the ideas of design and to find the potential binding modes. The successful design and computational studies led to the synthesis of bispyrimidine dione and tetrapyrimidine dione derivatives from uracil and aromatic aldehydes in the presence of HCl using novel methodology. The *in vitro* evaluation in HIV p24 assay revealed five potential uracil derivatives with IC_{50} values ranging from 191.5 μg ml^{-1} to 62.5 μg ml^{-1}. The *meta*-chloro substituted uracil compound **9a** showed promising activity with an IC_{50} value of 62.5 μg ml^{-1} which is well correlated with the computational studies. As expected, all the active compounds were noncytotoxic in BA/F3 and Mo7e cell lines highlighting the thoughtful design. The structure activity relationship indicates the position priority and lower log *P* values as the possible cause of inhibitory potential of the uracil compounds.

Received 16th April 2022
Accepted 29th May 2022

DOI: 10.1039/d2ra02450k

rsc.li/rsc-advances

1. Introduction

The evolution and pandemic of the Acquired Immune Deficiency Syndrome (AIDS) have been one of the greatest challenges faced by humankind. The first report of the disease came in the early 1980s, though it is widely accepted to have originated in the 1920s in Kinshasa.[1] The causative agent for the syndrome, the retrovirus Human T-lymphotropic virus type III (HTLV-III) was discovered in 1984 and was later renamed Human Immunodeficiency Virus (HIV) in 1986.[1] To date, HIV-AIDS continues to be a major public health concern without any major cure for the disease. This is reflected in the 2020 World Health Organisation report as 680 000 people died from AIDS and 1.5 million people were newly infected with HIV.[2] Two types of HIV (HIV-1 and HIV-2) have been recognized based on molecular and antigenic differences and among them, HIV-1 is more prevalent across the world.[1] AIDS is presently kept under control by highly active antiretroviral therapy (HAART) transforming the ailment from fatal infectious disease to controllable chronic affliction thereby reducing the mortality rate of HIV-positive patients. The current treatment for HIV through HAART targets diverse stages of the viral life cycle, especially two vital viral enzymes reverse transcriptase and protease. HAART has six major classes of drugs: Reverse Transcriptase (RT) inhibitors like Nucleoside RT inhibitors (NRTIs) and, non-nucleoside RT inhibitors (NNRTIs), integrase inhibitors (INIs), protease inhibitors (PIs), entry or fusion inhibitors (FIs), and chemokine receptor antagonists (CCR5 antagonists).[3] The cornerstone of HAART treatment is the co-administration of various drugs inhibiting HIV *via* different mechanisms of action. However, virologic failure is observed in patients receiving HAART in low-income countries.[4] Even with decreasing mortality rates, HAART is correlated with emerging drug resistance, which is attributed to high mutation rates of HIV-1 because of the error-prone nature of HIV-RT and its inability to proofread.[5]

Additionally, a numerous replication cycles occur in HIV-infected individuals thereby creating drug-resistant mutant strains of HIV.[6] These drug-resistant strains are also being passed between individuals, thus limiting the treatment options for even newly afflicted persons. The extended HAART treatment is also associated with toxicities like neuropathy, myopathy, hepatic steatosis as seen in NRTIs, drug hypersensitivities related with NNRTIs, and metabolic syndromes and diarrhoea from using PIs.[7] In this circumstance, there is an

[a]*Department of Chemistry, Pondicherry University, Kalapet, Puducherry-605014, India. E-mail: tharani.che@pondiuni.edu.in*

[b]*Department of Bioinformatics, Pondicherry University, Kalapet, Puducherry-605014, India*

[c]*Department of Microbiology, Pondicherry University, Kalapet, Puducherry-605014, India*

† Electronic supplementary information (ESI) available. CCDC 1946178. For ESI and crystallographic data in CIF or other electronic format see https://doi.org/10.1039/d2ra02450k

‡ Denotes equal contribution.

imperative need to find new anti-HIV drugs with an improved mechanism of action and novel targets in the HIV life cycle.

One suitable target is HIV-1 capsid protein (CA, p24) which is remarkably underexplored.

Capsid protein performs a vital role in HIV pathogenesis in the initial and late phases of the HIV lifecycle. The cone-shaped CA is released into cell cytosol after viral entry and disassembles, allowing reverse transcription and genome integration establishing HIV infection. The interaction of CA with Gag polyprotein during viral particle assembly results in the proteolytic cleavage, transforming the immature particles to mature virions forming viral RNA and other proteins.[8] As the CA is involved in multiple stages of viral replication, it can be an attractive antiviral target. CA inhibitors can bind to the capsid perturbing the stability of the protein and are also capable of interfering with the infection by competing for host factor binding.[9] CA is highly sensitive to mutations and has higher sequence conservation than other HIV proteins. The resistance of HIV to CA inhibitors requires mutations compromising the fitness of the virus, hence leading to a higher barrier to resistance and therapeutic efficiency.[10,11] So far, only a handful of capsid inhibitors are reported with benzodiazepine,[12] benzimidazole,[13] pyrrolopyrazolones,[14] furan,[15] and indole[16,17] scaffolds as in Fig. 1. However, there is no CA targeting compounds in clinical practice, and hence, a potential CA inhibitor holds promise for future drug development.

In drug development, the usage of small molecules is an efficient strategy considering the technical difficulties while employing other alternatives like short nucleotide segments or small peptides. Nucleosides and their corresponding nucleobases form major components in nucleic acids and bioactive systems, thus modifying their structure for drug development has a notable effect. Uracil is one such nucleobase, a naturally occurring pyrimidine, and can be a promising candidate as a CA inhibitor. Uracil can have a wide range of pharmaceutical properties depending on the substitution at N1, N3, C5, and C6 positions.[18] Uracil pharmacophore is well known in anti-cancer (5-fluorouracil, tegafur),[19] anti-herpes virus (trifluridine),[20] and antidiabetic (linagliptin and alogliptin) drugs.[21] The importance of the uracil scaffold in anti-HIV drugs is widely recognized with reports of uracil hybrid molecules as NNRTIs;[22–25] however, there is no commercial uracil-based CA inhibitor.

Considering the factor of cross-resistance in HIV drugs, it is essential to introduce new drugs to which the virus has never been exposed before. A set of compounds were designed by incorporating flexible and polar di-uracil moieties capable of efficient hydrogen bonding to develop novel CA inhibitors with potent anti-HIV activity. Molecular modelling techniques like molecular docking and molecular dynamics simulation were used for the efficient design of uracil derived CA inhibitors. The interactions and binding affinities of the designed compounds with CA were determined by molecular docking. Molecular dynamics simulations were further performed on superior complexes to validate the binding affinities and interactions.

The drug likeness of the compounds was taken into account before synthesis by considering their pharmacokinetic properties. Lipinski's rule of five was taken as the parameter for screening out compounds with poor absorption and

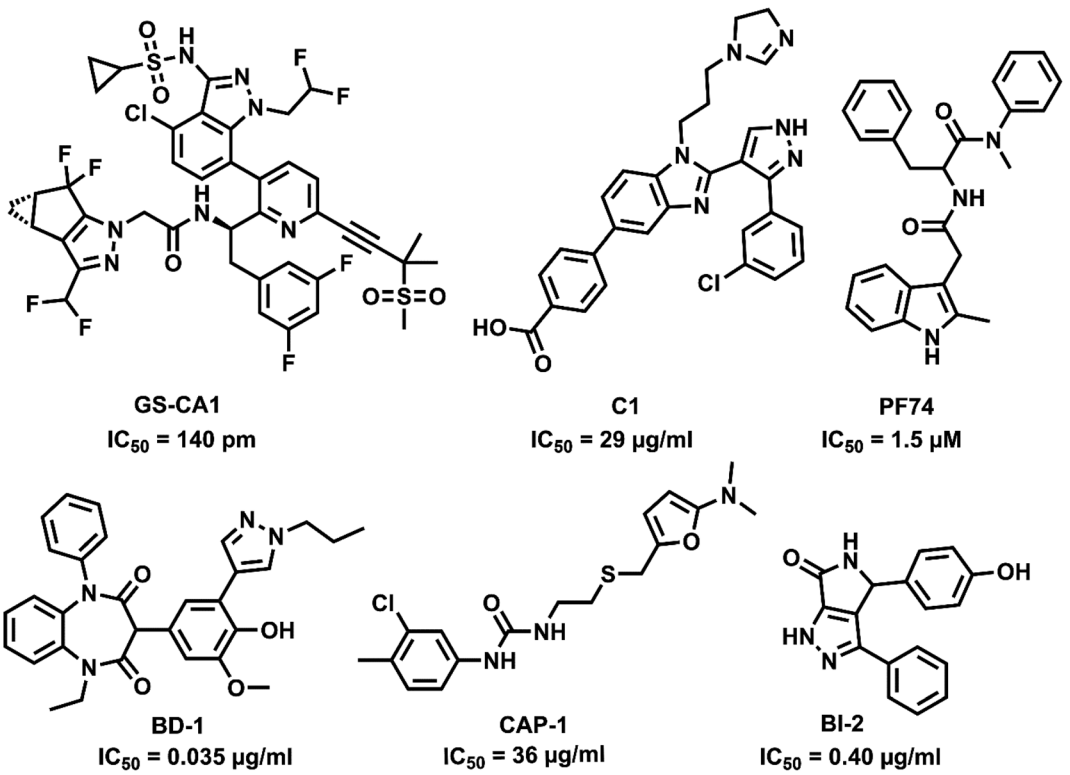

Fig. 1 Capsid inhibitors reported in the literature.

permeability. Additionally, the adsorption, distribution, metabolism, excretion, and toxicity (ADMET) properties were also considered as crucial pharmacokinetic features. The resulting compounds were successfully synthesized *via* novel synthetic methodology using moderate conditions and mild reagents. The biological assays like anti-HIV p24 assay and cytotoxicity studies of synthesized 5,5′-(phenylmethylene)bis(-pyrimidine-2,4(1*H*,3*H*)-dione) derivatives were carried out for further confirmation of computational observations and the results are discussed here.

2. Experimental section

2.1. Materials and methods

NMR spectra were recorded using 400 MHz (^{1}H NMR) and 101 MHz (^{13}C NMR) on a Bruker Avance-400 spectrometer. The chemical shifts are reported in ppm units with trimethyl silane as internal standard and *J* values are in hertz. Mass spectra were recorded using AGILENT Technologies 6530B Accurate Mass QTOF-LC/MS spectrometer. Fourier transform infrared (FT-IR) spectra were recorded on a Thermo Nicolet 6700 FT-IR spectrometer. Single crystal X-ray data were collected on Xcalibur Eos, Rigaku Oxford Diffraction instrument X-ray diffractometer with Mo-Kα radiation ($\lambda = 0.71073$ Å). Empirical absorption was done using SCALE3 ABSPACK scaling algorithm. The refinement was performed using XL, in the Olex 2-1.2 package and the structural solution by using SHELXS-97. The reagents and solvents were obtained from commercial sources and used by its very nature.

Dulbecco's Modified Eagle Medium (DMEM) media, Fetal Bovine Serum and antibiotic solution for p24 assay were obtained from Thermo Fischer Scientific, United States. German collection of microorganisms and animal cell cultures, DSMZ, Germany supplied Mo7e (ACC 104) and BA/F3 (ACC 300) cell lines. The cells were maintained in RPMI 1640 medium (Gibco, Waltham, MA USA) with 10% fetal calf serum (HiMedia, India) in the presence of 20 ng ml^{-1} human IL-3 and 10 ng ml^{-1} murine IL-3 (Peprotech Asia, Rehovot, Israel) respectively.

2.2. Docking studies

2.2.1 Enzyme–ligand docking. The monomer structure of HIV CA protein was obtained from the protein data bank (PDB). The protein–ligand docking study was performed using Schrödinger software suite. Protein was prepared using the protein preparation wizard module from Schrödinger software; in this module, protein was energy minimized, optimized, and any missing atoms/residues were added. To prepare the ligand for docking, the ligprep module was used; this module rectifies the Lewis structure of ligand. The receptor grid generation module was used to define the grid box of protein for further docking study. In the current study, active site residues were defined according to the reported crystal structure. Val-59, Gln-63, Met-66, Gln-67, Lys-70 were taken as active sites.[26] Protein–ligand interaction was performed using the glide module.

2.2.2. Molecular dynamics simulation. The complex which achieved the best score was selected for the simulation study; afterward, this protein–ligand complex was retrieved in .pdb format. The molecular dynamics simulation study was executed using GROMACS 5.1.4. The protein was first processed with the CHARMM27 force field in GROMACS 5.14, to generate a topology file for the protein. To obtain the topology file for ligand, ATB server was used,[27] the consequently processed ligand topology file was merged with protein topology file. The protein–ligand complex was packed inside a dodecahedron box of distance between side edge of box and protein set as 1.0 nm with SPC water model solvent molecule. The required amount of charge was added using 4 Cl^- ions to make the system neutral. Protein and protein–ligand complex minimized for 1000 steps with the steepest descent method. Consequently, a position restraint file for the ligand was generated and included in the main topology file. NPT and NVT equilibration were carried out for 1 ns. Berendsen-thermostat was employed in NPT and then NVT ensemble. The long-range electrostatic interaction was calculated using the particle mesh Ewald method. Finally, the MD simulation was executed for 100 ns. The bound conformation of **9a** with protein was checked for its binding energy using PRODIGY server post dynamics simulation.

2.3. General procedure for the synthesis of bis(pyrimidine-2,4(1*H*,3*H*)-diones), 1a–28a

Uracil (1 mmol for synthesizing compounds **1a–26a** and **28a** and 2 mmol for **27a**) in 5 ml water and 5 drops of conc. HCl (12 N) were taken in a round bottom flask and kept for stirring to initiate the reaction. After dissolution of uracil, the corresponding aldehyde was added slowly to the reaction mixture. The reaction mixture was refluxed for 6 hours at 70 °C and the progress of reaction was monitored by TLC (using ethyl acetate–hexane mixture). After completion, the mixture was cooled down to room temperature, poured into crushed ice, and neutralized by adding sodium bicarbonate solution (1 M) to allow precipitation. The resulting precipitate was filtered, washed with hot methanol to remove any aldehyde impurities and dried under vacuum to get compounds **1a–28a**.

2.4. General procedure for the synthesis of 5-(hydroxy(4-nitrophenyl)methyl)pyrimidine-2,4(1*H*,3*H*)-dione

Uracil (1 mmol) in 5 ml water and 5 drops of conc. HCl (12 N) were taken in an RB flask and kept for stirring to initiate the reaction. After dissolution of uracil, the corresponding aldehyde (1 mmol) was added slowly to the reaction mixture. The reaction mixture was refluxed for 4 hours at 70 °C and the progress of the reaction was monitored by TLC (using ethyl acetate–hexane mixture). After verifying the formation of the intermediate spot by TLC, the reaction mixture was cooled to room temperature and poured into crushed ice. The reaction mixture was neutralized by adding sodium bicarbonate solution (1 M) to allow precipitation. The resulting precipitate was filtered, washed with hot methanol to remove unreacted aldehyde impurities and dried under vacuum to get intermediate compound.

2.5. *In vitro* anti-HIV activity using the HIV-1 gag p24 inhibition assay

TZM-bl cells were plated at 1×10^4 cells per well in a 96 well plate and were incubated at 37 °C for 24 hours. The cells were infected with HIV-1 viral stocks at $TCID_{50}$ of 250 for preliminary screening and $TCID_{50}$ of 400 for IC_{50} determination. The viral stocks were later incubated with various concentrations of the samples (1 μg ml^{-1} for preliminary screening and varying concentrations for IC_{50} determination). The virus – sample complex was incubated at 37 °C for 5 days in CO_2 incubator. Following incubation, the cell supernatants were tested for the presence for HIV gap p24 core protein by HIV p24 ELISA kit (Xpress Bio, USA).

2.6. Statistical analysis

All results are expressed as mean ± S.D. and experiments were performed in triplicate. Values were compared using ANOVA by GraphPad Prism, version 5 (GraphPad Software, Inc., USA).

2.7. Cytotoxicity studies

Cell cytotoxicity assay was performed using WST-1 (Roche, Basel, Switzerland) according to manufacturer's protocol as given in ESI.†

3. Results and discussion

3.1. Molecular design

The studies show that the diarylpyrimidine derivatives are highly potent anti-HIV compounds[24,28] and hence we were curious if the introduction of alternate pharmacophores can produce compounds with compelling anti-HIV properties. The "four-point pharmacophore model" of existing diarylpyrimidines[24] consists of the hydrophobic region, the hydrogen bond interaction region, tolerant regions I and II (open towards solvent protein interface and is the most flexible region). The design of novel bis(pyrimidine-2,4(1*H*,3*H*)-diones) was inspired from this model, and modifications were applied to all regions for effective hydrogen bonding with the target as given in Fig. 2. Flexibility is one of the prominent features of HIV drugs, and hence we have incorporated phenyl ring with changeable substitutions. The change in substituents in the phenyl ring can improve the physicochemical properties of the designed compounds. The direct linkage of differently substituted phenyl rings to uracil moieties in the current scheme is maintained to investigate their viral potency. The hydrogen bonding of uracil moieties can offer better membrane permeability than other standard HIV inhibitors. The structures of all the designed compounds are given in Fig. 3.

The drug-like molecular properties of the compounds and ADMET properties were evaluated before molecular modelling studies for effectively screening out the compounds without drug like properties and the results are discussed in the following section.

3.2. Physicochemical properties of 5,5′-(phenylmethylene) bis(pyrimidine-2,4(1*H*,3*H*)-dione) derivatives

Drug likeness is an intricate balance of a wide range of molecular properties and structural features, namely, lipophilicity, H bonding, molecular size, electronic distribution, *etc.* determine if a compound is a drug or a non-drug. The presence of these pharmacophoric properties affects the behaviour of a compound within an organism in transportation, protein affinity, metabolic stability, and toxicity.[29] Even when absorption and bioavailability are two different parameters of the compound, the information regarding the absorption can help in designing the compounds with higher bioavailability. Lipinski's rule of five is a preliminary effort that helps to screen out the compounds with poor absorption and permeability[30,31] and the results are summarised in supplementary Table S1.†

Log *P* value determines the solubility and permeability of the compound which in turn affects absorption, a crucial factor for drug likeness. Drug candidates must possess required solubility to travel *via* the membrane without being trapped in them. The log *P* values of the drugs should be in the c log $P < 3$ range for

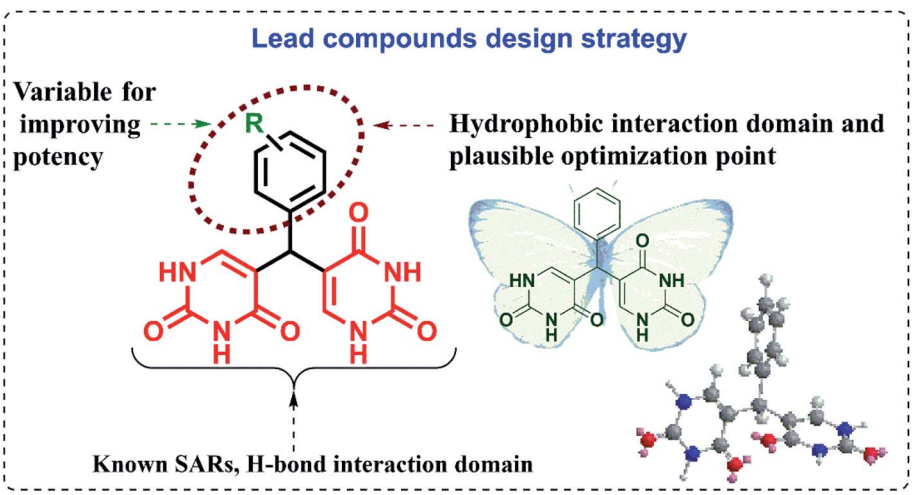

Fig. 2 The design strategy of lead compounds.

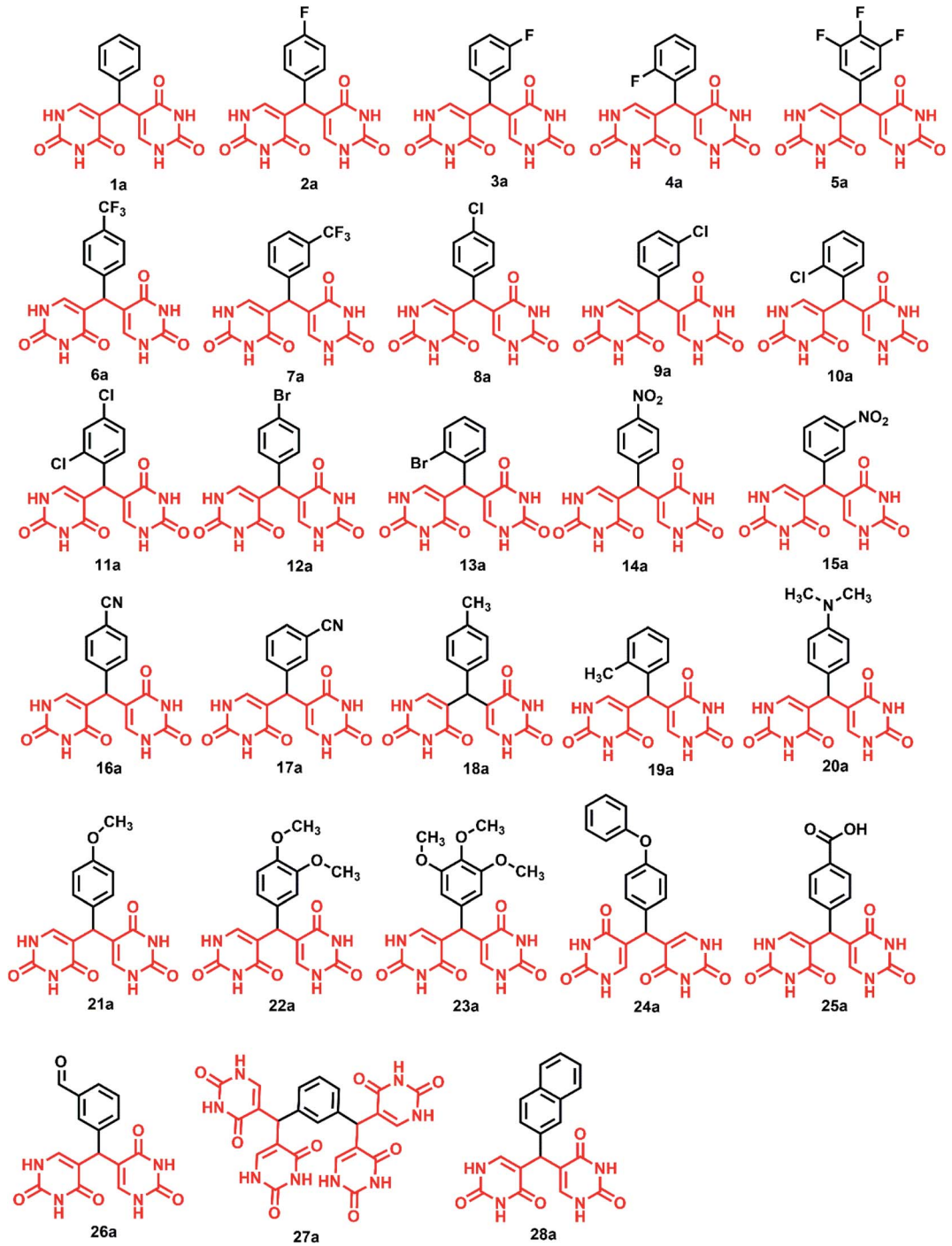

Fig. 3 Library of designed 5,5′-(phenylmethylene)bis(pyrimidine-2,4(1*H*,3*H*)-dione) derivatives.

better *in vivo* potency as well as for solubility.[32,33] All the designed compounds were found to have lower log *P* values indicating solubility and less toxicity. The positive log *P* values represents a liking for lipophilic environment and negative values denote a liking for hydrophilic or lipophobic environment.[34] Out of 28 compounds, 17 compounds showed negative log *P* values indicating their lipophobic nature. Moving on to molecular weight as a crucial parameter, except **27a**, the molecular weights of all the compounds were in the allotted range of below 500 falling in line with Lipinski's rules. However, with molecular weights below 1000 Da, all these compounds can also be classified under small molecules,[35] having several advantages like predictable pharmacokinetics and pharmacodynamics properties, easy manufacture, higher stability and bioavailability.[36] These compounds have plentiful NH and OH groups capable of donating H-bonds along with C=O groups to accept incoming bonds and are expected to have a momentous impact on interacting proteins and nucleic acids *via* H-bonding.

The compounds can thereby be stabilised within the binding pockets of the biological target due to H-bonding ability.[37] Hence, 5,5′-(phenylmethylene)bis(pyrimidine-2,4(1*H*,3*H*)-dione) derivatives were designed by considering the number of H-donors and acceptors. As per Lipinski's rule, except 4 compounds, all the remaining derivatives showed H-bonding within the accepted range. The rotatable bond count is the measure of molecular flexibility which along with total polar surface area predicts good oral bioavailability. Higher bioavailability is the measure of designing compounds as good therapeutic agents.[38] The increased number of rotatable bonds has negative effect on membrane permeability and surprisingly all the designed 5,5′-(phenylmethylene)bis(pyrimidine-2,4(1*H*,3*H*)-dione) derivatives have rotatable bonds in the 2–6 range which is acceptable by Veber's rule. Total polar surface area (TPSA) is correlated to the compound's physicochemical properties in terms of toxicities. Compounds with lower TPSA values have adverse toxicities as they can easily cross the cellular membranes and get distributed into tissues. Compounds with low-C log *P*/high-TPSA are likely to be 2.5 times cleaner than toxic.[33] All the compounds possess high TPSA values from 131.45 to 262.90, eradicating the hypothesis that low TPSA increases the binding of compounds to off-targets.[33] As per the drug likeness rules, 5,5′-(phenylmethylene)bis(pyrimidine-2,4(1*H*,3*H*)-dione) derivatives showed drug like molecular properties and were further evaluated for their respective Absorption, Distribution, Metabolism, Excretion, and Toxicity (ADMET) properties.

3.3. ADMET properties of 5,5′-(phenylmethylene) bis(pyrimidine-2,4(1*H*,3*H*)-dione) derivatives

Most of the potential drug candidates in *in vitro* studies fail in further drug development stages due to their efficacy and safety profile, highlighting that ADMET properties (as given in Table S1†) play a vital role in drug design. Solubility is one of the basic requirements of an orally administrated drug, and higher lipophilicity impacts the aqueous solubility. The optimal drug solubility is higher than -4 log mol L^{-1}, and all the designed compounds showed solubility higher than -3 log mol L^{-1}. The ability for absorption determines the oral bioavailability and hence it is important to screen the compounds for intestinal permeability before synthesis. The human colon adenocarcinoma (Caco-2) cell line has morphological and functional similarities with human enterocytes, thereby making that a favoured model to estimate the permeability of drug candidates in high throughput screening. As required, all the derivatives showed higher permeability than the optimal value of -5.15.[39] As the intestine is the primary absorption site, the percentage of absorption of the compounds was estimated. Except for two compounds (**25a** and **27a**), all the derivatives showed absorption similar to or higher than C1.

The volume of distribution (V_D) of the compounds was evaluated and higher V_D shows drug distribution in tissues. Log $V_D < -0.15$ is considered lower and except **28a**, all other compounds are better distributed in plasma than tissues. The fraction unbound of all the compounds was lower and in the range of reference drugs indicating that the compounds can be diffused to cellular membranes. Like reference drugs, the designed compounds were blood–brain barrier (BBB) impermeable as they displayed log BBB < -0.1. The cytochromes are responsible for the biotransformation of most of the foreign objects and hence the metabolism of the designed compounds by cytochromes were evaluated *in silico*. Majority of designed compounds were identified as substrates and/or inhibitors of CYP3A4 and CYP1A2. The study is beneficial as it predicts whether parallel administration of compounds with a known CYP substrate can alter drug disposition, toxicity or efficacy.[40] The total clearance, oral rat toxicity and hepatotoxicity, were also considered parameters for drug design.

3.4. *In silico* studies

Prior to synthesis, the compounds were explored *via in silico* analysis to validate the drug design for p24 protein. Molecular docking studies against HIV CA were carried out followed by molecular dynamic simulation studies for the most promising compounds.

3.4.1. Molecular docking. HIV CA plays vital role in the initial and late stages of viral replication and is often regarded as one of the prominent therapeutic targets. The conformational changes within CA triggers its assembly into a conical protein shell named capsid, which encloses viral genome and viral enzymes. The inhibition of proper assembly can reduce viral infectivity.[15] Potential HIV CA inhibitors from within the designed library of compounds were identified using molecular docking techniques. Understanding the target protein and any potential binding sites is required to analyse the inhibitory potential of the small molecule library. Retroviral CA proteins are extraordinarily preserved with approximately 70% sequence preservation within viral mutants.[41] The viral CA monomer has two domains, the N terminal domain (NTD) and C terminal domain (CTD) which in HIV-1 includes residues 1–145 and 150–231 respectively.[41] The NTD of a monomeric CA interacts with the NTD's of 5 other CA to form one CA-hexamer.[41–43] CA-hexamers connect with neighbouring hexamers *via* homodimer linkages between CTD's thus, allowing for lattice formation.[41–43] Inter hexamer CA NTD–CTD interactions also help to stabilize the capsid. The mature capsid consists of hundreds of CA-hexamers forming the bulk of the lattice and, a few CA-pentamers at lattice closure points.[41–43] Disruption at any one of these critical junctures would inhibit capsid formation.[26,44–50] The work by V. Lee *et al.* has been instrumental in capsid inhibition computational studies, our approach is not quite as in depth as we expect to compare *in silico* with *in vitro*.[50] Thus, HIV-1 CA monomer (PDB: 2XDE) was chosen as a potential target as it is the smallest building block with a crystal structure of acceptable quality that we can target for capsid inhibition.

The binding pockets for both NTD and CTD are well documented.[26,44–48,50] CTD binding pocket residues include Arg173, Gln179, Lys182, Tyr169 and Leu172.[46–48,50] NTD binding pocket contains numerous important residues including, Asn53, Leu56, Asn57, Thr58, Val59, Gln63, Met66, Gln67, Leu69, Lys70, Ile73, Tyr130, Ala105 and Thr107.[46–48,50] The results of the

docking study were extremely promising as all members of the library had multiple interactions within the NTD binding pocket. All compounds showed hydrophobic interactions within the NTD pocket.

All the compounds except **1a**, **27a** and **17a**, showed one or more H-bonds with residues from Asn57 to Lys70. Asn57 interaction in particular is a highly conserved residue for CA intra-hexamer NTD–NTD hydrogen bond network.[41] Glide-Scores of compounds were compared to identify which is most promising, more negative glidescores correspond with better binding bearing in mind that there are no absolute good or Glidescores only relative comparisons to be made. **9a** was most promising (as given in Fig. 4) with its glidescore of -6.41 kcal mol^{-1} but compounds **7a**, **10a**, **1a**, **24a** and **3a** were the next most promising based on their binding scores between -5.52 kcal mol^{-1} to -4.99 kcal mol^{-1}. The remaining compounds had glidescores between -4.02 kcal mol^{-1} and -4.91 kcal mol^{-1}. Molecular dynamics simulations were performed to understand the stability of the protein-ligand complex of **9a** and HIV CA monomer due to **9a** having the highest GlideScore.

3.4.2. Molecular dynamics simulations. The docking studies revealed the prime candidate **9a** from the compound library based on binding energy and interactions as shown in Table 1.

The hydrogen bond interaction of HIV-1 CA monomer with compound **9a** is shown in Fig. 4. The interactions of **9a** with HIV-1 CA monomer has a -6.41 kcal mol^{-1} glidescore which is significantly better than the second highest interacting agent compound **7a** at -5.52 kcal mol^{-1}. Residues Val59, *Gln67*, and *Lys70* were observed to form hydrogen bonds with compound **9a**. These amino acid residues are found in the R3 pocket of the protein molecule. The R3 pocket plays a vital role in forming a bridge between the NTD of one HIV CA monomer and the CTD of another monomer.[41,42] This indicates that ligand molecule bound to active site amino acid residues, may hinder the HIV-1 capsid assembly. The conformations over time of protein and protein–ligand complex were compared by generating the root means square deviation (RMSD) plot as shown in Fig. 5c. RMSD is coarse method to note deviation of conformation or change in physical location in comparison to an initial state. In the current study, protein alone does not undergo significant conformational changes as indicated by the RMSD and finds relatively stability at an early stage and does not deviate much for the remainder of the simulation without much fluctuation. On the other hand, the protein-ligand complex shows higher fluctuation and is less rigid than the protein alone. The RMSD of the protein indicates relative stability from 25 ns to 100 ns. In the case of the protein–ligand complex, the RMSD value fluctuates markedly throughout the simulation. The protein–ligand complex achieves relative stability from 80 ns to 100 ns when compared to the first 80 ns wherein the fluctuations were much higher. This graph suggests the compound **9a** has a profound impact on protein conformation and stability. The root means square fluctuation (RMSF) graph is a coarse method that allows us to observe which amino acid residues deviate from their position during simulation. The RMSF plot shows residue numbers 75 to 100 of protein–ligand complex deviate greatly as shown in Fig. 5d. This is significant as the active site of the protein exists between the residues 75 to 100. The ligand significantly disrupted the active site residues when compared with simulation of protein alone. The radius of gyration of only protein maintains a constant size throughout simulation, whereas, for the protein–ligand complex the radius of gyration fluctuates in size within the 0.5 nm range as shown in Fig. 5a. This result indicates compound **9a** has a mild effect on change in overall protein size. The plot of solvent-accessible surface area (SASA) in Fig. 5b shows that in protein–**9a** complex SASA has overall decreased in comparison with simulation of plain protein. The lower SASA is a direct result of compound **9a** being present in the binding site cavity. This lower accessibility of solvent to the binding cavity may be detrimental as water

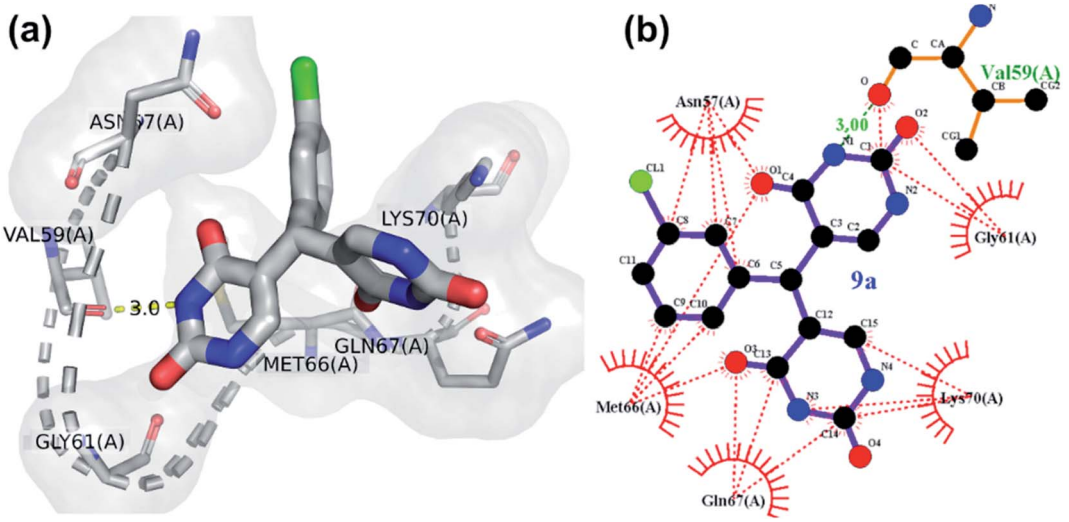

Fig. 4 Binding interaction of compound **9a** with HIV-CA (a) 3D diagram (b) ligplot diagram.

Table 1 Glide scores and amino acid interactions with HIV-1 CA monomer

Compound code	Glidescore (kcal mol^{-1})	Interacting residues[a] H bond interactions (Bond length in Å)	Hydrophobic interactions
1a	−5.26	—	***Met66***, **Gln63**, **Ile73**, ***Leu56***, ***Lys70***, **Asn57**
2a	−4.46	**Val59** (3.02)	***Met66***, ***Lys70***, ***Gln67***, **Asn57**, Gly61, **Val59**
3a	−4.99	**Val59** (2.85), ***Met66*** (2.78)	***Lys70***, ***Leu56***, **Leu69**, **Ile73**, **Asn57**, Gly61, **Gln63**, **Val59**, ***Met66***
4a	−4.46	Gly61 (3.06), **Gln63** (2.83)	***Met66***, **Asn57**, ***Leu56***, Gly60, **Val59**, ***Gln67***, **Gln63**, Gly61
5a	−4.60	***Gln67*** (2.80), **Val59** (2.89)	***Met66***, ***Lys70***, **Asn57**, **Val59**, ***Gln67***
6a	−4.91	Gly61 (2.84), **Gln63** (2.96), **Val59** (3.22)	***Gln67***, **Asn57**, ***Met66***, Gly60, **Gln63**, **Val59**, Gly61
7a	−5.52	***Gln67*** (3.03), **Asn57** (3.01)	***Met66***, **Asn57**, **Gln63**, ***Gln67***
8a	−4.61	Gly61 (3.22, 2.96), **Gln63** (2.88)	***Met66***, ***Leu56***, **Asn57**, ***Gln67***, Gly60, Gly61, **Gln63**
9a	−6.41	**Val59** (3.00)	***Met66***, ***Gln67***, ***Lys70***, Gly61, **Asn57**, **Val59**
10a	−5.31	**Asn57** (2.95), **Val59** (2.94), Gly61 (2.85)	***Lys70***, ***Met66***, Gly60, **Gln63**, ***Gln67***, **Val59**, Gly61, **Asn57**
11a	−4.54	Gly61 (2.87, 2.82)	***Met66***, **Asn57**, ***Leu56***, **Gln63**, Gly60, Gly61
12a	−4.49	Gly61 (2.76, 2.96), **Gln63** (2.88)	***Met66***, **Asn57**, ***Leu56***, ***Gln67***, Gly60, **Gln63**, Gly61
13a	−4.32	**Asn57** (2.96), **Val59** (2.96), Gly61 (2.88)	***Met66***, Gly60, **Gln63**, ***Lys70***, ***Gln67***, **Asn57**, **Val59**, Gly61
14a	−4.37	Gly61 (2.76, 3.11), **Gln63** (3.03)	***Met66***, ***Leu56***, **Asn57**, Gly60, ***Gln67***, Gly61, **Gln63**
15a	−4.58	**Val59** (2.99), Gly61 (3.02), ***Lys70*** (3.05)	***Met66***, Gly60, Gly67, **Asn57**, **Val59**, Gly61, **Gln63**
16a	−4.30	**Val59** (3.22), Gly61 (2.86), **Gln63** (3.03)	***Met66***, Gly60, Gly67, ***Leu56***, **Asn57**, **Val59**, Gly61, **Gln63**
17a	−4.17	**Val59**, Gly61, **Gln63**, ***Gln67***, ***Lys70***	—
18a	−4.53	Gln57 (3.03), **Val59** (2.86)	Gln57, **Val59**, **Tyr130**, **Asn53**, ***Leu56***, ***Met66***, **Asn57**, ***Lys70***
19a	−4.66	**Val59** (2.98), Gly61 (2.90), **Asn57** (3.01)	Gly60, ***Leu56***, ***Lys70***, ***Met66***, ***Gln67***, **Gln63**, **Val59**, Gly61, **Asn57**
20a	−4.43	***Lys70*** (3.08), ***Gln67*** (2.78)	***Lys70***, ***Gln67***, Gly60, **Val59**, **Gln63**, **Asn57**, **Asn53**, ***Leu56***, **Ile73**, ***Met66***, **Tyr130**
21a	−4.61	Gly61 (2.93, 3.32), **Gln63** (2.83), **Val59** (3.08)	***Gln67***, ***Leu56***, **Asn57**, ***Met66***, Gly60, Gly61, **Gln63**, **Val59**
22a	−4.43	**Val59** (3.00), ***Gln67*** (3.02)	**Gln63**, ***Leu56***, **Asn57**, ***Lys70***, **Asn53**, **Leu69**, ***Met66***, ***Gln67***, **Val59**
23a	−4.21	***Gln67*** (2.92)	**Asn57**, **Val59**, **Asn53**, ***Lys70***, **Leu69**, ***Met66***, **Gln63**, ***Gln67***
24a	−5.15	Gly61 (2.77, 3.14)	Gly60, ***Leu56***, **Asn57**, **Ile73**, **Asn53**, **Tyr130**, ***Met66***, **Gln63**, ***Gln67***, Gly61
25a	−4.72	**Asn57** (3.12), **Val59** (2.75), **Gln63** (3.03), ***Met66*** (2.87)	***Leu56***, Gly60, **Gln63**, ***Met66***, **Asn57**, **Val59**
26a	−4.02	Gly61 (2.99), **Val59** (2.84), ***Lys70*** (3.15)	Gly60, **Gln63**, ***Gln67***, **Asn57**, ***Met66***, **Val59**, Gly61
27a	−4.50	—	**Asn53**, **Asn57**, **Val59**, Gly61, **Gln63**, ***Met66***, ***Gln67***, ***Lys70***, **Tyr130**
28a	−4.20	***Gln67*** (2.91), **Val59** (2.72)	***Met66***, ***Leu56***, **Asn57**, ***Lys70***, ***Gln67***, **Val59**

[a] Key pocket residues are marked in bold letters. Residues capable of drug-resistance related mutations are given in italic and bold letters.[48] H-bonds between 2.7 Å to 3.35 Å and hydrophobic contacts between 2.90 Å and 3.90 Å were considered.

molecules present in the binding site are known to help stabilize HIV capsid conformations.[41] The binding energy of **9a** post dynamics simulation as obtained from PRODIGY server analysis was −6.4 kcal mol^{-1}.[51]

3.5. Chemistry

The promising results from *in silico* studies led us to proceed with the synthesis of designed compounds. The synthesis involving uracil and benzaldehyde in literature ended up with a mixture of 5-(chloro(phenyl)methyl)pyrimidine-2,4(1*H*,3*H*)-dione and bis(pyrimidine-2,4(1*H*,3*H*)-diones).[52] The isolation of bis(pyrimidine-2,4(1*H*,3*H*)-diones) as major product was unreported and this prompted us to delve deeper to design the synthetic strategy for these compounds as depicted in Scheme 1. Here, the reaction between differently substituted aldehydes and uracil in 1 : 1 ratio in H_2O with conc. HCl as catalyst at 70 °C yielded novel 5,5′-(phenylmethylene)bis(pyrimidine-2,4(1*H*,3*H*)-dione) derivatives. The novel bis pyrimidinedione derivatives having both hydrophilic and lipophilic groups did not undergo any further reactions and were stable. The optimization of reaction conditions is given in Table S2.† For understanding the structure–activity relationships (SARs), numerous substituted bis pyrimidine derivatives (**1a–28a**) were prepared. In an analogous approach, 5,5′,5″,5‴-(1,3-phenylenebis(methanetriyl)) tetrakis(pyrimidine-2,4(1*H*,3*H*)-dione) (**27a**) was synthesized. Here, **27a** was synthesized using the same reaction conditions from isophthalaldehyde and uracil in 1 : 2 ratio.

The uracil derivatives so formed were characterised by spectroscopic techniques. In all the compounds, the characteristic peak of the bis(pyrimidine-2,4(1*H*,3*H*)-diones) derivatives appears as singlet around 5–6 ppm in ^{1}H Nuclear Magnetic Resonance (NMR) spectra and around 35–50 ppm in ^{13}C NMR spectra, occasionally merging with DMSO septet. The NH protons of uracil appear as singlets around 10–11 ppm in ^{1}H NMR spectra and C=O peaks of uracil appear at 160–163 ppm in ^{13}C NMR spectra. The experimental and theoretical molecular weights show exact likeness in mass spectra indicating the formation of expected product.

3.6. Mechanistic considerations

In case of reaction between uracil and 4-nitro benzaldehyde (Scheme 1), initially 5-(hydroxy(4-nitrophenyl) methyl) pyrimidine-2,4(1*H*,3*H*)-dione was isolated along with the expected product. The structure of intermediate compound in Fig. 6b was

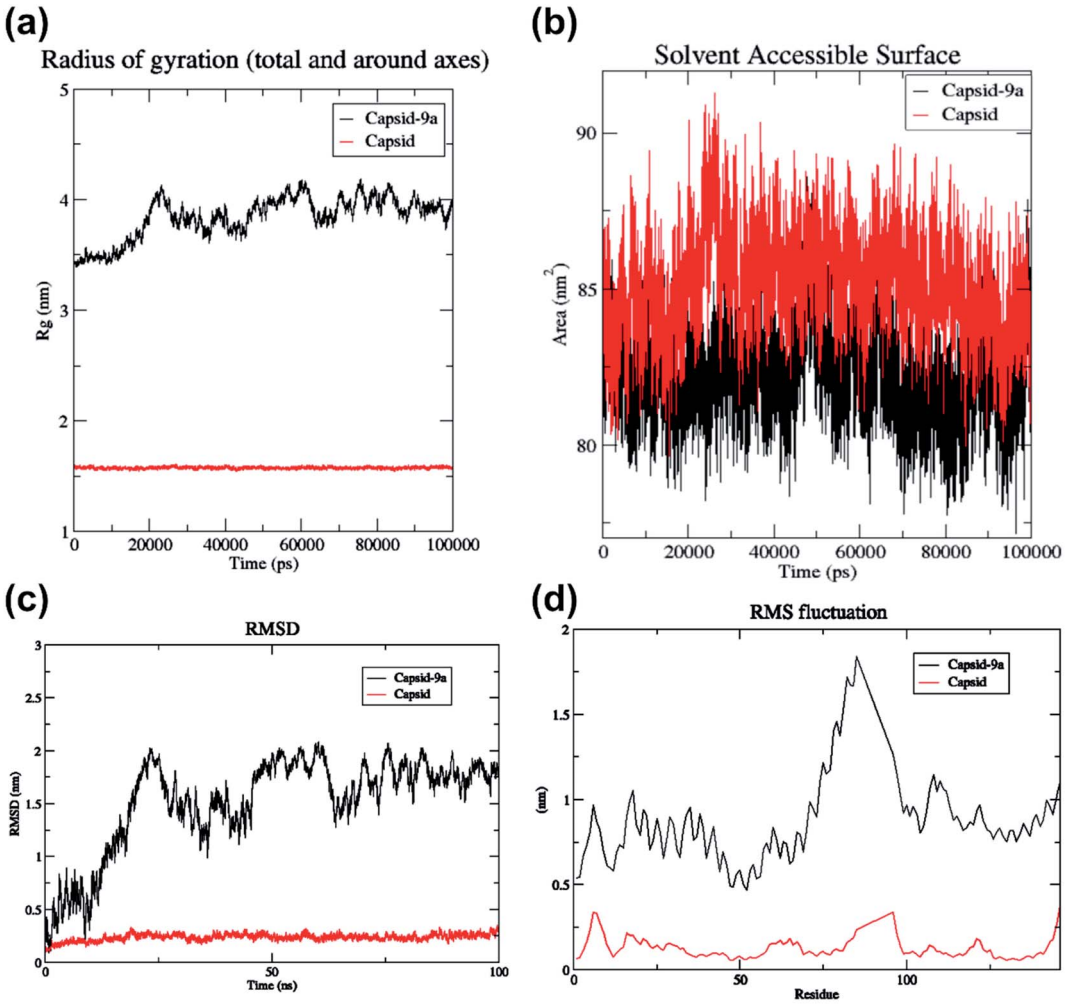

Fig. 5 Data obtained from molecular dynamics simulation of HIV-1 CA monomer with compound **9a**.

confirmed by NMR spectra and single crystal XRD data. The characteristic hydroxy peak of the intermediate appears as a singlet at 4.5 ppm merging with solvent water peaks. The CH protons resonate at 5.59 ppm and the uracil NH peaks appear at 10–11 ppm in ^{1}H NMR spectra. Moving on to ^{13}C NMR spectra, C–OH peak appears at 67.12 ppm and C=O peaks appear around 150–163 ppm. The experimental and theoretical molecular weights show exact likeness indicating the formation of intermediate compound. To verify the role of the isolated intermediate, further reaction of this compound with uracil was carried out as per standardised reaction conditions. The reaction proceeded to form 5,5′-((4-nitrophenyl) methylene) bis(-pyrimidine-2,4(1*H*,3*H*)-dione), which was yet again characterised by spectroscopic techniques. The previously reported formation of 5-(chloro(phenyl)methyl)pyrimidine-2,4(1*H*,3*H*)-dione[52] was not observed and this led us to develop a plausible mechanism for the reaction as given in Fig. 6a. The synthetic protocol involves the activation of carbonyl compound by the acid catalyst followed by initial nucleophilic addition of uracil to form the intermediate. After the formation of intermediate, the reaction may proceed *via* unimolecular substitution. The 5-(hydroxy(4-nitrophenyl) methyl) pyrimidine-2,4(1*H*,3*H*)-dione intermediate was isolated as the chance of formation of intermediate is higher since the benzylic carbocation is becoming less stable due to the presence of electron withdrawing nitro group at para position.

The protonation of the intermediate and subsequent S_N1 reaction forms the resultant bis(pyrimidine-2,4(1*H*,3*H*)-diones). All the aforementioned derivatives were purified by washing with hot methanol resulting in the isolation of desired products, the structures were assigned based on spectral data and analytical evidences.

3.7. Crystallisation of 5-(hydroxy(4-nitrophenyl)methyl) pyrimidine-2,4(1*H*,3*H*)-dione and structure determination

The intermediate 5-(hydroxy(4-nitrophenyl)methyl)pyrimidine-2,4(1*H*,3*H*)-dione (given in Fig. 6b) was isolated in the reaction between uracil and 4-nitro benzaldehyde. The intermediate was washed with hot methanol to remove any unreacted aldehyde impurities before crystallization. The final pure compound was dissolved in minimal amount of DMSO and crystallized at room temperature. The XRD data are summarised in Table S3† and single crystal XRD diagram of intermediate (CCDC Number:

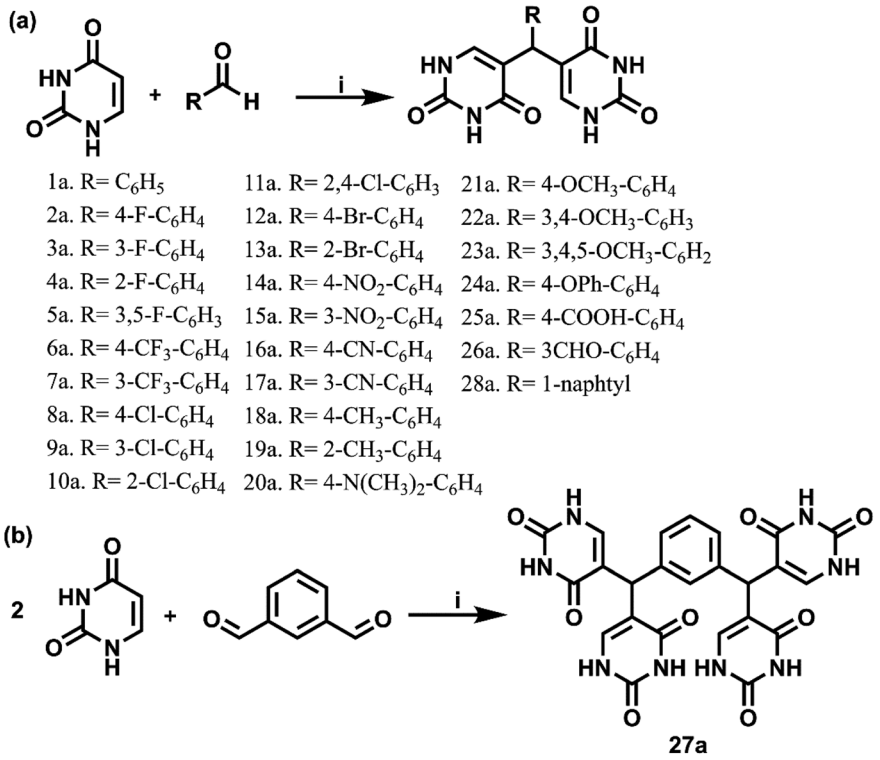

Scheme 1 (a) Synthesis of bis(pyrimidine-2,4(1*H*,3*H*)-diones). (b) Synthesis of 5,5′,5″,5‴-(1,3-phenylenebis(methanetriyl))tetrakis(pyrimidine-2,4(1*H*,3*H*)-dione).

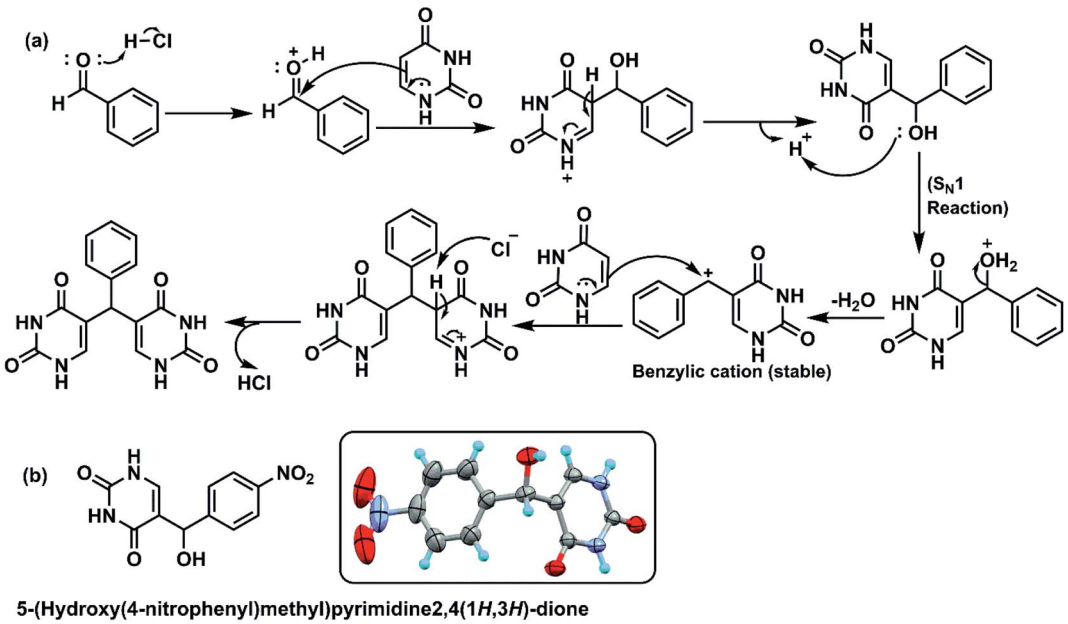

Fig. 6 (a) Plausible reaction mechanism of formation of bis(pyrimidine-2,4(1*H*,3*H*)-dione) derivatives, (b) structure of an isolated intermediate.

1946178) is given in Fig. 7. Here, two molecules of intermediate interacted *via* two C═O and NH bonds of uracil moiety. This is in accordance with the reported H-bonding interactions in uracil.[53] The H-bonding stabilizes the crystal structure. However, the free hydroxy group in intermediate compound did not participate in H bonding. The packing diagram reveals the presence of 5-(hydroxy(4-nitrophenyl)methyl)pyrimidine-2,4(1*H*,3*H*)-dione in the corners.

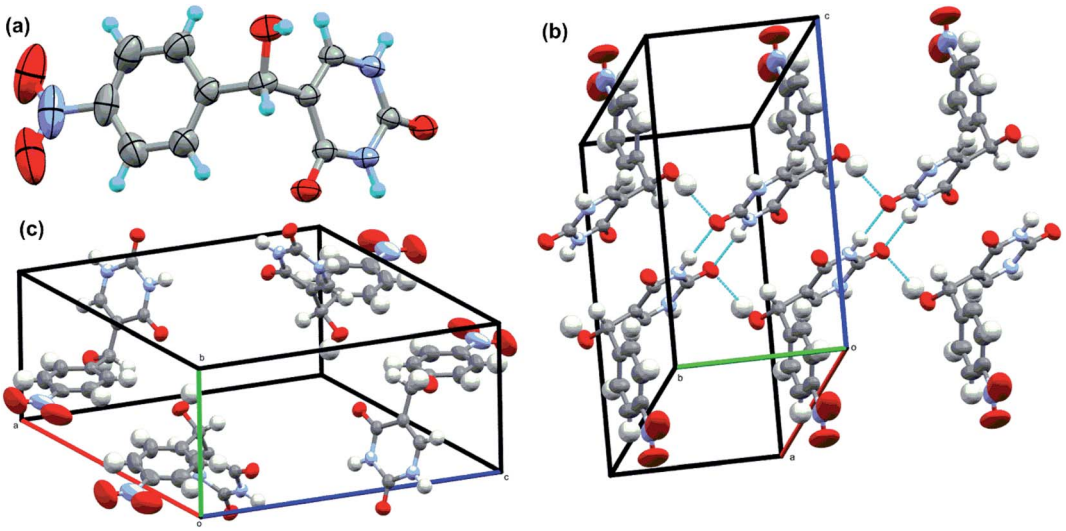

Fig. 7 Single-crystal XRD data. (a) The ORTEP diagram, (b) hydrogen bond interaction diagram and (c) packing diagrams of intermediate compound in Fig. 6.

3.8. Biological evaluation

3.8.1. Effect of bis(pyrimidine-2,4(1*H*,3*H*)-diones) on HIV-1 p24 antigen production. The current study aims at the molecular modelling studies, successful synthesis and further biological evaluation of the novel bis(pyrimidine-2,4(1*H*,3*H*)-diones) by systematic modification of the compounds for exploring the structure activity relationships (SARs). The modifications involved in this library include (a) the presence of uracil dimers for plausible H bonding with the target, (b) use of the variable hydrophobic domain for enhanced lipophilicity and (c) incorporation of bioisostere for effective SARs. The successfully synthesized and isolated bis pyrimidines prompted us to test the anti-HIV activity of the derivatives against HIV-1 Subtype C using azidothymidine (AZT) as a standard drug.

To explore anti-HIV-1 activity, 1 μg ml^{-1} of bis(pyrimidine-2,4(1*H*,3*H*)-diones) were initially tested against activated PBMC infected with 250 $TCID_{50}$ of a lab adapted strain of HIV-1C as given in Fig. 8. The detailed results are given in Table S4.† In the preliminary screening at 1 μg ml^{-1}, five compounds showed promising activity with percentage inhibition varying from 58% (**9a**) to 74% (**7a**). Most of the compounds gave less than 20% inhibition and the modifications seem to render the bis(pyrimidine-2,4(1*H*,3*H*)-diones) inactive towards HIV-p24. However, out of 5 compounds showing promising activity, four compounds were halogen derivatives. Compared to other derivatives, the higher activity of halogens may be due to their high lipophilic nature which readily allows them to pass through the lipid layers of the viral membranes. This is well connected with the use of halogen bonding in HIV drug development as they can avoid the risks of emerging drug resistance.[54] The preliminary active compounds were further screened for their cytotoxicity before with IC_{50} determination.

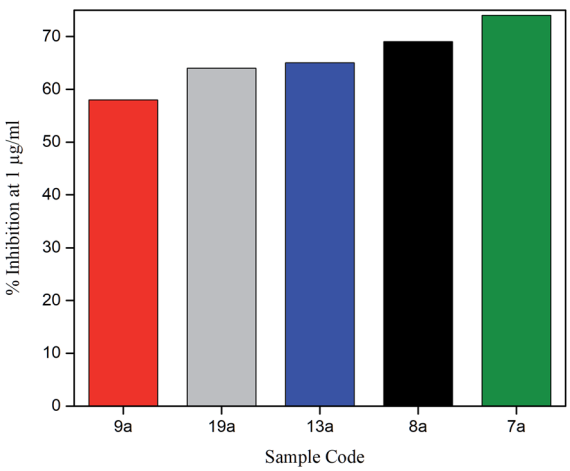

Fig. 8 Effect of bis(pyrimidine-2,4(1*H*,3*H*)-diones) on HIV-1 p24 antigen production at 1 μg ml^{-1}.

3.9. Evaluation of cytotoxicity of promising compounds

Cytotoxicity of compounds **7a**, **8a**, **9a**, **13a** and **19a** were tested in human megakaryocyte cell line (Mo7e) and Murine pro B cell line (BA/F3). Compounds inhibiting greater than 50% of cell growth were considered cytotoxic. When treated with 1 μg ml^{-1} of **7a**, **8a**, **9a**, **13a** and **19a**, more than 90% of viability in Mo7e cells was observed. Similarly, we observed more than 90% viability in Mo7e cells treated with 5 μg ml^{-1} of all the compounds except **9a** and **19a**. Also, in BA/F3, cell viability of more than 90% was visible when treated with 1 μg ml^{-1} and 5 μg ml^{-1} of compounds **7a**, **8a**, **9a**, **13a** and **19a**. Overall our results suggest that 1 μg ml^{-1} concentration of compounds **7a**, **8a**, **9a**, **13a** and **19a** are not cytotoxic to Mo7e and BA/F3 cells as given in Fig. 9.

3.10. Evaluation of IC_{50} values of active compounds against p24 of HIV-1C

The inhibitory effect of the five active bis(pyrimidine-2,4(1*H*,3*H*)-diones) were further evaluated by HIV-p24 assay with 400 $TCID_{50}$ of HIV-1C. The higher virus concentration was

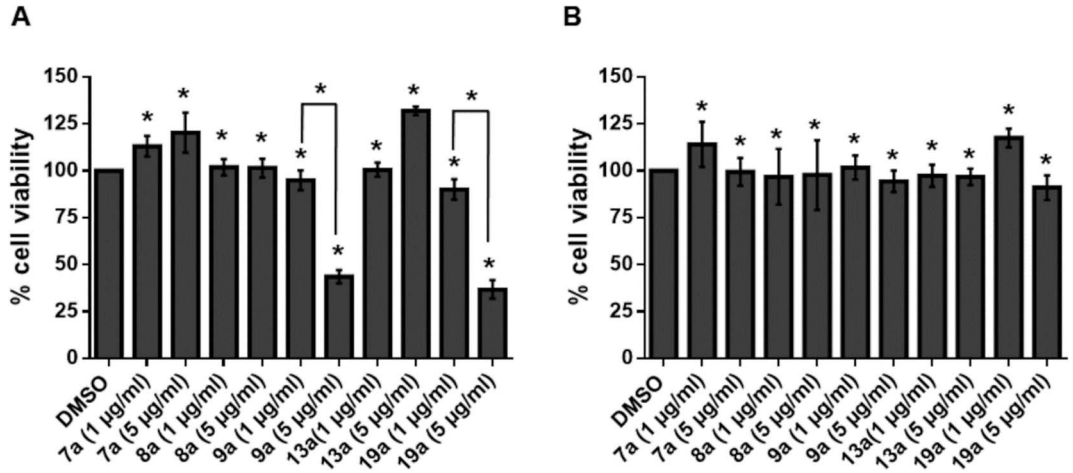

Fig. 9 Percentage cell viability of Mo7e and BA/F3 against **7a**, **8a**, **9a**, **13a** and **19a**. (A) Mo7e cells and (B) BA/F3 cells were stimulated with indicated concentrations of **7a**, **8a**, **9a**, **13a** and **19a** for 24 hours. Data are represented as mean ± s.e.m. *P* value is calculated using Student's *t*-test. $^{*}P < 0.05$.

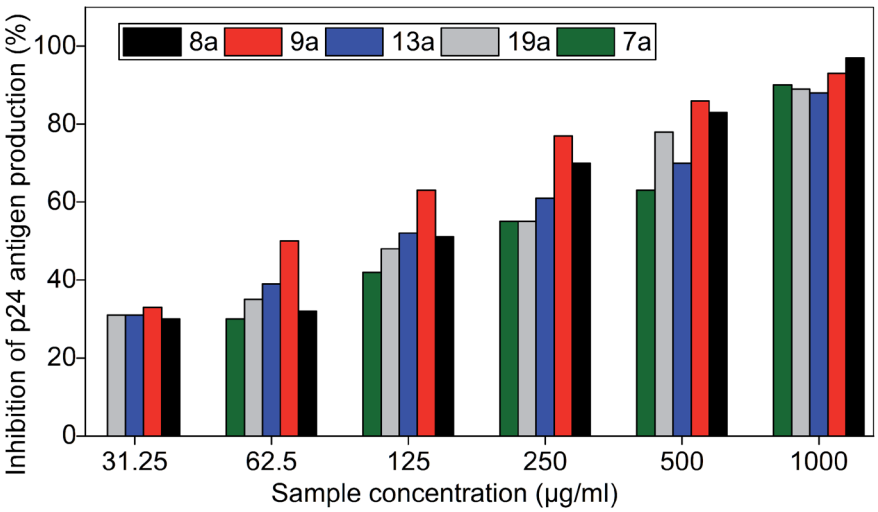

Fig. 10 Inhibition of p24 of HIV-1C by bis(pyrimidine-2,4(1*H*,3*H*)-diones). Azidothymidine (AZT) was used as positive control and virus control was 1×10^4 PFU ml^{-1}. The data shown is the mean ± S.D. of three independent experiments represented in percentage of inhibition.

deliberately selected, and the IC_{50} of the compounds were evaluated *in vitro* and results are summarised in Fig. 10 and Table S5.†

IC_{50} values of the compounds are as follows: **7a** (191.5 μg ml^{-1}), **8a** (120.5 μg ml^{-1}), **9a** (62.5 μg ml^{-1}), **13a** (112.4 μg ml^{-1}), and **19a** (152.4 μg ml^{-1}).

All the compounds which gave promising inhibition in preliminary studies are biologically and chemically diverse. The structure–activity relationships of the compounds are discussed in detail here. Most of the active compounds were halogen derivatives indicating that the functional group may play a role in the anti-HIV activity. However, the location of various halogens also influenced the anti-HIV activity with the compounds exhibiting multiple levels of potencies against HIV-1C with IC_{50} values ranging from 191.5 μg ml^{-1} to 62.5 μg ml^{-1}. Compounds **8a**, **9a** and **13a** were characterised by the presence of mono-halogen substituents like Cl and Br. Compared to the non-substituted **1a** and other mono-halogen substitutions (**2a**, **3a**, **4a**, **10a**, and **12a**), the presence of Cl and Br substitutions is favourable for HIV-1C inhibition as seen from the *in vitro* studies. Surprisingly, F-substitutions (**2a**, **3a** and **4a**) made the compounds inactive against the pathogen, contrary to the reported works as most of the HIV drugs have F-derivatives. Notably, *meta*-Cl substitution (**9a**) with IC_{50} value of 62.5 μg ml^{-1} was necessary for the enhancement of anti-HIV activity when compared to the other substitutions. The higher activity of **9a** may be due to lower log *P* value and meta effect of the substituent. Meta substitution with a non-flat substituent like Cl can enhance the aqueous solubility without affecting the lipophilicity, thereby improving the biological activity.[55] The presence of *para*-Cl substitution in **8a** drastically changed the IC_{50} value to 120.5 μg ml^{-1} while *ortho*-Cl in **10a** was inactive

against HIV-1C. However, reverse trend was observed for bromo substitutions as *para*-Br substitution in **12a** was inactive when compared to *ortho*-Br substitution in **13a**.The latter displayed an IC_{50} value of 112.4 μg ml^{-1}. The better activity of **13a** may be credited to its lower log *P* value indicating higher lipophilicity to permeate through viral cell membranes. Compounds **5a** and **11a** were characterised by disubstituted halogens and seemed to be unfavourable for anti-HIV activity as compared to monovalent analogues. For compounds bearing halogens, the position priority as observed from IC_{50} values are, meta > ortho > para as in the case of the compounds **9a** > **13a** > **8a**.

For compounds **14a–17a**, strong electron withdrawing groups like NO_2 and CN seems to negatively affect the inhibitory potential of HIV-1C. In contrast, introducing an electron donating group like methyl derivative showed potent anti-HIV activity. However, considering the positions of the methyl derivatives, the IC_{50} values varied sharply with *ortho*-methyl substitution (**19a**) having an IC_{50} value of 152.5 μg ml^{-1} while *para*-methyl substitution (**18a**) remained inactive. Trifluoromethyl substitutions (**6a** and **7a**) were also introduced as they are versatile groups in medicinal chemistry. However, it was not contributing much to the activity with **7a** giving an IC_{50} value of 191.5 μg ml^{-1} while **6a** was inactive. The compounds with *N*-methyl substitution (**20a**) and methoxy substitutions (**21a**, **22a** and **23a**) were inferior to methyl substitution. Replacing the methoxy substitution with phenoxy (**24a**), phenyl ring with naphthyl (**28a**) or the introduction of aldehyde substitution in various equivalence to form **26a** and **27a** or the use of carboxylic acid substituent (**25a**) did not affect the activity.

From the discussions it can be concluded that the position of the functional groups and log *P* values of the compounds decide the activity. Interestingly, all the active compounds were monovalent bioisostere of either H or Br. The hydrophobicity of the compounds also helped in bioactivity as they can easily penetrate through the lipid bilayer of HIV. The studies indicate the possibility of using halogen derivatives for further modifications of the pyrimidine for enhanced activity.

4. Conclusion

A series of uracil derivatives were carefully designed based on the existing four-point pharmacophore model as effective capsid protein inhibitors. The design strategy involves the incorporation of flexible and polar di-uracil moieties capable of efficient hydrogen bonding and considering lipophilic substituents for easier membrane penetration. This is in line with the emerging cross-resistance in HIV drugs. The compounds designed showed drug-like properties and were initially docked with HIV capsid protein monomer to find the potential binding modes. Molecular dynamic simulations were performed for one of the most promising compound **9a** to explain structural changes of the systems. The RMSD and RMSF plots indicated significant structural alteration of HIV-1 CA monomer when complexed with compound **9a**. The promising *in silico* results led us to the *in vitro* evaluation of compounds in HIV p24 assay which revealed five potential compounds with an IC_{50} values ranging from 191.5 μg ml^{-1} to 62.5 μg ml^{-1}. The *meta*-chloro substituted **9a** displayed promising activity with an IC_{50} value of 62.5 μg ml^{-1} which correlates well with the theoretical studies. The active compounds were noncytotoxic in BA/F3 and Mo7e cell lines highlighting the thoughtful design. The structure–activity relationship indicates the position priority and lower log *P* values as the possible cause of inhibitory potential of the compounds.

Author contributions

DR: conceptualization, methodology, investigation and writing – original draft AD: conceptualization, methodology and investigation. AKM and SKM: formal analysis, investigation and writing original draft (Carried out molecular docking and dynamic simulation studies for HIV CA protein). BVG: writing – review & editing (Data interpretation for computational studies), writing original draft and visualization. AS and MM: formal analysis, investigation, writing original draft (carried out the cytotoxicity studies for compounds). KT: resources, supervision, writing – review & editing, project administration and funding acquisition.

Funding

Deepthi Ramesh is the recipient of DST for DST-INSPIRE fellowship (SRF). Prof. Tharanikkarasu Kannan received financial support from University Grants Commission (UGC), New Delhi under Special Assistance Program, stage DSA-I to Department of Chemistry, Pondicherry University (No. F.540/6/DSA-1/2016/(SAP-1) dated 31-10-2018).

Conflicts of interest

There are no conflicts to declare.

Acknowledgements

Authors thank Prof. M. Elanchezhiyan and Jerusha Daniel, Dept. of Microbiology, University of Madras, Chennai, India, for anti-HIV studies on consultancy basis. The authors are grateful for Central Instrumentation Facility (CIF), Pondicherry University for spectral analysis. The authors also thank Prof. Binoy K. Saha, Dr Arijit Saha and Dr Sharada Durgam, Department of Chemistry, Pondicherry University for XRD characterization. Authors thank Debayan Chattopadhyay, Department of Chemistry, Pondicherry University for timely help.

Notes and references

1 C. J. P. R. Ananthanarayan, *Ananthanarayan and Paniker's Textbook of Microbiology*, University Press, 10th edn, 2017.
2 *Global progress report on HIV, viral hepatitis and sexually transmitted infections, Accountability for the global health sector strategies 2016–2021: actions for impact*, World Health Organization, Geneva, 2021, Licence: CC BY-NC-SA 3.0 IGO.

3 R. Romeo, D. Iannazzo, L. Veltri, B. Gabriele, B. Macchi, C. Frezza, F. Marino-Merlo and S. V. Giofrè, *Molecules*, 2019, **24**, 1718.
4 J. C. Reed, D. Solas, A. Kitaygorodskyy, B. Freeman, D. T. B. Ressler, D. J. Phuong, J. V. Swain, K. Matlack, C. R. Hurt, V. R. Lingappa and J. R. Lingappa, *J. Virol.*, 2021, **95**, e00883-20.
5 J. D. Roberts, K. Bebenek and T. A. Kunkel, *Science*, 1988, **242**, 1171.
6 J. M. Coffin, *Science*, 1995, **267**, 483.
7 S. Redshaw and M. Westby, *Expert Opin. Emerging Drugs*, 2001, **6**, 209–224.
8 S. A. Ali, S.-Y. Teow, T. C. Omar, A. S.-B. Khoo, T. S. Choon and N. M. Yusoff, *PLoS One*, 2016, **11**, e0145986.
9 S. K. Carnes, J. H. Sheehan and C. Aiken, *Curr. Opin. HIV AIDS*, 2018, **13**, 359–365.
10 G. Li, J. Verheyen, S. Y. Rhee, A. Voet, A. M. Vandamme and K. Theys, *Retrovirology*, 2013, **10**, 126.
11 S. J. Rihn, S. J. Wilson, N. J. Loman, M. Alim, S. E. Bakker, D. Bhella, R. J. Gifford, F. J. Rixon and P. D. Bieniasz, *PLoS Pathog.*, 2013, **9**, e1003461.
12 L. D. Fader, R. Bethell, P. Bonneau, M. Bös, Y. Bousquet, M. G. Cordingley, R. Coulombe, P. Deroy, A. M. Faucher, A. Gagnon, N. Goudreau, C. Grand-Maître, I. Guse, O. Hucke, S. H. Kawai, J. E. Lacoste, S. Landry, C. T. Lemke, E. Malenfant, S. Mason, S. Morin, J. O'Meara, B. Simoneau, S. Titolo and C. Yoakim, *Bioorg. Med. Chem. Lett.*, 2011, **21**, 398–404.
13 M. Tremblay, P. Bonneau, Y. Bousquet, P. DeRoy, J. Duan, M. Duplessis, A. Gagnon, M. Garneau, N. Goudreau, I. Guse, O. Hucke, S. H. Kawai, C. T. Lemke, S. W. Mason, B. Simoneau, S. Surprenant, S. Titolo and C. Yoakim, *Bioorg. Med. Chem. Lett.*, 2012, **22**, 7512–7517.
14 L. Lamorte, S. Titolo, C. T. Lemke, N. Goudreau, J. F. Mercier, E. Wardrop, V. B. Shah, U. K. von Schwedler, C. Langelier, S. S. Banik, C. Aiken, W. I. Sundquist and S. W. Mason, *Antimicrob. Agents Chemother.*, 2013, **57**, 4622–4631.
15 B. N. Kelly, S. Kyere, I. Kinde, C. Tang, B. R. Howard, H. Robinson, W. I. Sundquist, M. F. Summers and C. P. Hill, *J. Mol. Biol.*, 2007, **373**, 355–366.
16 S. Rankovic, R. Ramalho, C. Aiken, I. Rousso and F. Kirchhoff, *J. Virol.*, 2018, **92**, e00166-21.
17 T. Kobayakawa, M. Yokoyama, K. Tsuji, M. Fujino, M. Kurakami, S. Boku, M. Nakayama, M. Kaneko, N. Ohashi, O. Kotani, T. Murakami, H. Sato and H. Tamamura, *Biomolecules*, 2021, **11**, 208.
18 A. Pałasz and D. Cież, *Eur. J. Med. Chem.*, 2015, **97**, 582–611.
19 K. Miura, M. Kinouchi, K. Ishida, W. Fujibuchi, T. Naitoh, H. Ogawa, T. Ando, N. Yazaki, K. Watanabe, S. Haneda, C. Shibata and I. Sasaki, *Cancers*, 2010, **2**, 1717–1730.
20 A. A. Carmine, R. N. Brogden, R. C. Heel, T. M. Speight and G. S. Avery, *Drugs*, 1982, **23**, 329–353.
21 N. Li, L.-J. Wang, B. Jiang, S.-J. Guo, X.-Q. Li, X.-C. Chen, J. Luo, C. Li, Y. Wang and D.-Y. Shi, *Bioorg. Med. Chem. Lett.*, 2018, **28**, 2131–2135.
22 P. Ordonez, T. Hamasaki, Y. Isono, N. Sakakibara, M. Ikejiri, T. Maruyama and M. Baba, *Antimicrob. Agents Chemother.*, 2012, **56**, 2581.
23 X. Wang, J. Zhang, Y. Huang, R. Wang, L. Zhang, K. Qiao, L. Li, C. Liu, Y. Ouyang, W. Xu, Z. Zhang, L. Zhang, Y. Shao, S. Jiang, L. Ma and J. Liu, *J. Med. Chem.*, 2012, **55**, 2242–2250.
24 H. Zhang, Y. Tian, D. Kang, Z. Huo, Z. Zhou, H. Liu, E. De Clercq, C. Pannecouque, P. Zhan and X. Liu, *Eur. J. Med. Chem.*, 2017, **130**, 209–222.
25 M. V. Putz, N. A. Duda□ and A. Isvoran, *Int. J. Mol. Sci.*, 2015, **16**, 19553–19601.
26 L. Wang, M. C. Casey, S. K. V. Vernekar, R. L. Sahani, J. Kankanala, K. A. Kirby, H. Du, A. Hachiya, H. Zhang, P. R. Tedbury, J. Xie, S. G. Sarafianos and Z. Wang, *Eur. J. Med. Chem.*, 2020, **204**, 112626.
27 A. K. Malde, L. Zuo, M. Breeze, M. Stroet, D. Poger, P. C. Nair, C. Oostenbrink and A. E. Mark, *J. Chem. Theory Comput.*, 2011, **7**, 4026–4037.
28 L.-Q. Sun, L. Zhu, K. Qian, B. Qin, L. Huang, C. H. Chen, K.-H. Lee and L. Xie, *J. Med. Chem.*, 2012, **55**, 7219–7229.
29 J. V. Turner and S. Agatonovic-Kustrin, in *Comprehensive Medicinal Chemistry II*, ed. J. B. Taylor and D. J. Triggle, Elsevier, Oxford, 2007, pp. 699–724, DOI: **10.1016/B0-08-045044-X/00147-4**.
30 C. A. Lipinski, *Drug Discovery Today: Technol.*, 2004, **1**, 337–341.
31 C. A. Lipinski, F. Lombardo, B. W. Dominy and P. J. Feeney, *Adv. Drug Delivery Rev.*, 1997, **23**, 3–25.
32 K. D. Freeman-Cook, R. L. Hoffman and T. W. Johnson, *Future Med. Chem.*, 2013, **5**, 113–115.
33 J. D. Hughes, J. Blagg, D. A. Price, S. Bailey, G. A. DeCrescenzo, R. V. Devraj, E. Ellsworth, Y. M. Fobian, M. E. Gibbs, R. W. Gilles, N. Greene, E. Huang, T. Krieger-Burke, J. Loesel, T. Wager, L. Whiteley and Y. Zhang, *Bioorg. Med. Chem. Lett.*, 2008, **18**, 4872–4875.
34 V. Khanna and S. Ranganathan, *BMC Bioinf.*, 2009, **10**(Suppl 15), S10.
35 K.-H. Thierauch, in *Encyclopedia of Cancer*, ed. M. Schwab, Springer Berlin Heidelberg, Berlin, Heidelberg, 2011, pp. 3448–3451, DOI: **10.1007/978-3-642-16483-5_5374**.
36 H. X. Ngo and S. Garneau-Tsodikova, *MedChemComm*, 2018, **9**, 757–758.
37 J. Kostal, in *Advances in Molecular Toxicology*, ed. J. C. Fishbein and J. M. Heilman, Elsevier, 2016, vol. 10, pp. 139–186.
38 D. F. Veber, S. R. Johnson, H.-Y. Cheng, B. R. Smith, K. W. Ward and K. D. Kopple, *J. Med. Chem.*, 2002, **45**, 2615–2623.
39 N.-N. Wang, J. Dong, Y.-H. Deng, M.-F. Zhu, M. Wen, Z.-J. Yao, A.-P. Lu, J.-B. Wang and D.-S. Cao, *J. Chem. Inf. Model.*, 2016, **56**, 763–773.
40 S. F. Zhou, *Curr. Drug Metab.*, 2008, **9**, 310–322.
41 A. T. Gres, K. A. Kirby, V. N. Kewal Ramani, J. J. Tanner, P. Owen and S. G. Sarafianos, *Science*, 2015, **349**, 99–104.

42 O. Pornillos, B. K. Ganser-Pornillos, B. N. Kelly, Y. Hua, F. G. Whitby, C. D. Stout, W. I. Sundquist, C. P. Hill and M. Yeager, *Cell*, 2009, **137**, 1282–1292.
43 B. K. Ganser-Pornillos, A. Cheng and M. Yeager, *Cell*, 2007, **131**, 70–79.
44 B. N. Kelly, S. Kyere, I. Kinde, C. Tang, B. R. Howard, H. Robinson, W. I. Sundquist, M. F. Summers and C. P. Hill, *J. Mol. Biol.*, 2007, **373**, 355–366.
45 K. Singh, F. Gallazzi, K. J. Hill, D. H. Burke, M. J. Lange, T. P. Quinn, U. Neogi and A. Sonnerborg, *Front. Microbiol.*, 2019, **10**, 1227.
46 X. Jiang, G. Wu, W. A. Zalloum, M. E. Meuser, A. Dick, L. Sun, C. H. Chen, D. Kang, L. Jing, R. Jia, S. Cocklin, K. H. Lee, X. Liu and P. Zhan, *RSC Adv.*, 2019, **9**, 28961–28986.
47 L. Sun, T. Huang, A. Dick, M. E. Meuser, W. A. Zalloum, C. H. Chen, X. Ding, P. Gao, S. Cocklin, K. H. Lee, P. Zhan and X. Liu, *Eur. J. Med. Chem.*, 2020, **190**, 112085.
48 J. O. Link, M. S. Rhee, W. C. Tse, J. Zheng, J. R. Somoza, W. Rowe, R. Begley, A. Chiu, A. Mulato, D. Hansen, E. Singer, L. K. Tsai, R. A. Bam, C. H. Chou, E. Canales, G. Brizgys, J. R. Zhang, J. Li, M. Graupe, P. Morganelli, Q. Liu, Q. Wu, R. L. Halcomb, R. D. Saito, S. D. Schroeder, S. E. Lazerwith, S. Bondy, D. Jin, M. Hung, N. Novikov, X. Liu, A. G. Villasenor, C. E. Cannizzaro, E. Y. Hu, R. L. Anderson, T. C. Appleby, B. Lu, J. Mwangi, A. Liclican, A. Niedziela-Majka, G. A. Papalia, M. H. Wong, S. A. Leavitt, Y. Xu, D. Koditek, G. J. Stepan, H. Yu, N. Pagratis, S. Clancy, S. Ahmadyar, T. Z. Cai, S. Sellers, S. A. Wolckenhauer, J. Ling, C. Callebaut, N. Margot, R. R. Ram, Y. P. Liu, R. Hyland, G. I. Sinclair, P. J. Ruane, G. E. Crofoot, C. K. McDonald, D. M. Brainard, L. Lad, S. Swaminathan, W. I. Sundquist, R. Sakowicz, A. E. Chester, W. E. Lee, E. S. Daar, S. R. Yant and T. Cihlar, *Nature*, 2020, **584**, 614–618.
49 F. Ternois, J. Sticht, S. Duquerroy, H. G. Krausslich and F. A. Rey, *Nat. Struct. Mol. Biol.*, 2005, **12**, 678–682.
50 H. A. A. Karim, T. Rungrotmongkol, S. M. Zain, N. A. Rahman, C. Tayapiwattana and V. Lee, *J. Mol. Liq.*, 2019, **277**, 63–69.
51 R. V. Honorato, P. I. Koukos, B. Jiménez-García, A. Tsaregorodtsev, M. Verlato, A. Giachetti, A. Rosato and A. M. J. J. Bonvin, *Front. Mol. Biosci.*, 2021, **8**, 729513.
52 L. Spáčilová, P. Džubák, M. Hajdúch, S. Křupková, P. Hradil and J. Hlaváč, *Bioorg. Med. Chem. Lett.*, 2007, **17**, 6647–6650.
53 L. Bencivenni, F. Ramondo, A. Pieretti and N. Sanna, *J. Chem. Soc., Perkin Trans. 2*, 2000, 1685–1693, DOI: **10.1039/B002342F**.
54 Z. Xu, Z. Yang, Y. Liu, Y. Lu, K. Chen and W. Zhu, *J. Chem. Inf. Model.*, 2014, **54**, 69–78.
55 Y. Ichikawa, M. Hiramatsu, Y. Mita, M. Makishima, Y. Matsumoto, Y. Masumoto, A. Muranaka, M. Uchiyama, Y. Hashimoto and M. Ishikawa, *Org. Biomol. Chem.*, 2021, **19**, 446–456.